journal

J. Am. Ceram. Soc., 75 [4] 822–29 (1992)

Control of Grain-Boundary Pinning in Al_2O_3/ZrO_2 Composites with Ce^{3+}/Ce^{4+} Doping

Liang A. Xue,* Karsten Meyer, and I-Wei Chen*

Department of Materials Science and Engineering, The University of Michigan, Ann Arbor, Michigan 48109

The control of the microstructure of Ce-doped Al_2O_3/ZrO_2 composites by the valence change of cerium ion has been demonstrated. Two distinctively different types of microstructure, large Al_2O_3 grains with intragranular ZrO_2 particles and small Al_2O_3 grains with intergranular ZrO_2 particles, can be obtained under identical presintering processing conditions. At doping levels greater than ~3 mol% with respect to ZrO_2, Ce^{3+} raises the alumina grain-boundary to zirconia particle mobility ratio. This causes the breakaway of grain boundary from particles and the first type of microstructure. On the other hand, Ce^{4+} causes no breakaway and produces a normal intergranular ZrO_2 distribution. The dramatic effect of Ce^{3+} on the relative mobility ratio is found to be associated with fluxing of the glassy boundary phase and is likewise observed for other large trivalent cation dopants. The ZrO_2 second phase acts as a scavenger for these trivalent cations, provided their solubility limit in ZrO_2 is not exceeded. [Key words: grain growth, alumina, zirconia, ceria, dopants.]

I. Introduction

SECOND-PHASE pinning can be used to inhibit grain growth in ceramics.[1-3] When the maximum permissible velocity (V_p) of the particle is greater than or equal to that of the grain boundary (V_b), the particle stays on the grain boundary and exerts a pinning effect on the grain boundary. This gives rise to a fine-grained microstructure with intergranular second-phase particles, schematically shown in Fig. 1(A). On the other hand, when $V_p < V_b$, second-phase particles break away from the grain boundary. The pinning effect is then lost, resulting in a large-grained microstructure with intragranular second-phase particles, schematically shown in Fig. 1(B). Since V_p and V_b are, respectively, proportional to the particle mobility, M_p, and grain-boundary mobility, M_b, the control of grain growth and especially of abnormal grain growth in a two-phase system translates directly to the control of the relative mobility M_p/M_b. A large M_p/M_b ratio will produce situation A in Fig. 1, whereas a small ratio will result in situation B.

One way to control M_p/M_b is to change the size of the second-phase particle, r, to exploit the scaling relation, $M_p \propto r^{-n}$ where $n = 3$ or 4, depending on whether volume diffusion or interfacial diffusion dominates material transport across the particle.[4] This method has its practical limitation: particles with a size much smaller than 0.1 μm are difficult to produce and process. Another way to control the mobility ratio is by doping. Doping may introduce lattice defects or alter grain-boundary characteristics which in turn affect the diffusion process and both M_p and M_b. This is practiced in sintering, where the pinning particles are pores. A classic example is found in alumina, where a fine-grained dense microstructure can be obtained by MgO doping.[2,5-6]

A technically important ceramic composite system, ZrO_2-toughened Al_2O_3 (ZTA), where ZrO_2 is the second phase, has been chosen in the present work to study the doping effect. Exaggerated grain growth of this system has been reported in the past by several groups.[3,7-11] In contrast to those studies, which have made no systematic attempt to examine the dopant effect, cerium has been selected as the dopant in our investigation. The special feature of cerium as a dopant is that its valence state can be easily controlled through the use of different sintering atmospheres; it is in the Ce^{+4} state in an oxidizing atmosphere and the Ce^{3+} state in a reducing atmosphere.[12,13] This special feature has proved advantageous in that it produced drastically different microstructures despite identical presintering processing conditions. The results also reveal a special role of the zirconia second phase as a scavenger for some impurities. Lastly, the effect of processing-introduced glass-forming impurities will be discussed.

II. Experimental Procedure

High-purity powders of Al_2O_3 (AKP-50, >99.99%, particle size ~0.2 μm, Sumitomo Chemical America, Inc., NY) and ZrO_2 (TZ-0, 99.98%, particle size ~0.1 μm, Tosoh USA, Inc., Atlanta, GA) were used as the starting materials. The zirconia powder was first dispersed ultrasonically in distilled water with a surfactant (Darvan 821A, R.T. Vanderbilt Co., Norwalk, CT). Doping was achieved by adding an aqueous solution of $Ce(NO_3)_3$ to the zirconia slurry. The pH of the mixture was

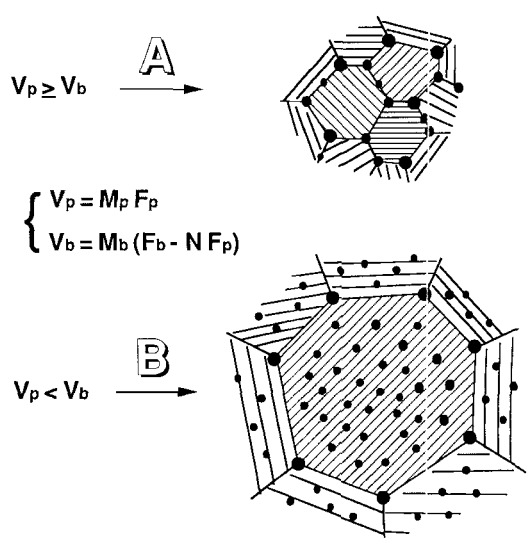

Fig. 1. Schematic of grain-boundary–second-phase particle interactions. (See Ref. 2.)

G. L. Messing—contributing editor

Manuscript No. 196355. Received September 17, 1991; approved December 19, 1991.
Supported by the U.S. Department of Energy (BES) under Grant No. DE-FG02-87ER45302.
*Member, American Ceramic Society.

then adjusted to floc the suspension. The slurry was dried and calcined at 1000°C for 30 min. The doped powder was again dispersed and mixed with alumina powder and the surfactant in distilled water, then attrition milled in an alumina jar using zirconia balls. The mixed slurry was pressure cast under 1 MPa into cakes, as described elsewhere.[14] These cakes were dried, isostatically cold pressed at 400 MPa, and calcined at 700°C for 30 min. Sintering was conducted at 1550°C in either an oxidizing (air for maintaining Ce^{4+}) or reducing (hydrogen for maintaining Ce^{3+}) atmosphere for a time up to 4 h. Samples reached relative densities greater than 98% in about 15 min at the sintering temperature.

The sintered samples were polished and thermally etched at 1450°C for 5 min. Microstructures of the samples were examined by SEM. The alumina grain size was obtained by multiplying the average linear length of at least 400 grains by 1.56 and was corrected for the zirconia second-phase content.[15] Zirconia particle size was also measured, using average values of 200 particles.

The volume fractions of zirconia second phase studied were 2%, 5%, and 10%. The level of Ce doping, as a molar ratio Ce/(Ce + Zr), is expressed in percentage, ranging from 1% to 10% in most cases. The notation adopted for denoting the compositions, such as 95A/5Zr10Ce, stands for 95 vol% Al_2O_3 and 5 vol% $Zr_{0.9}Ce_{0.1}O_{2-x}$ and the Ce doping level in this example will be referred to as 10%. In the above expression, x is a number dependent on the valence of Ce.

In addition to the above, other compositions of various alumina/zirconia composites have also been studied. These include the Al_2O_3/CeO_{2-x} system (without ZrO_2), the $Al_2O_3/MO_{1.5}$ system (with M being Y^{3+} and La^{3+} but without ZrO_2), and a series of high-purity $Al_2O_3/MO_{1.5}$ systems in which processing-related impurity contamination has been largely avoided. The processing procedures of the latter are described in Sections III(3) and III(4).

III. Results

(1) Microstructural Effect of Ce Doping and Sintering Atmosphere

The microstructure of sample 98A/2Zr3Ce sintered for 4 h in air is compared with that sintered in hydrogen in Fig. 2. The air-sintered sample shows normal grain growth of moderate grain sizes and mostly (white) intergranular zirconia second-phase particles. The hydrogen-sintered sample, however, shows abnormal grain growth and predominantly (white) intragranular zirconia particles. These microstructural features shown in Fig. 2 are very much analogous to those schematically drawn in Fig. 1. Thus, two distinctively different types of microstructure were obtained from the same starting material under identical processing conditions before firing, through the control of the sintering atmosphere.

The breakaway phenomenon observed is attributed to Ce doping. Samples of various zirconia volume fractions without Ce doping show no breakaway during sintering in either hydrogen or air. In Fig. 3 the grain size and particle size data for undoped alumina/zirconia samples during hydrogen sintering are plotted as a function of sintering time. A microstructure of uniformly small grains with fine intergranular ZrO_2 particles was always observed. This changes with Ce doping. After sintering for 4 h, the alumina grain sizes for two zirconia volume fractions (2 vol% and 10 vol%) are shown in Fig. 4 as a function of Ce content. When sintered in air, the grain size remains almost unchanged at both Zr contents. In hydrogen sintering, on the other hand, the grain size increases rapidly with Ce content. Also note that the alumina grain size of 90A/10Zr is always smaller than that of 98A/2Zr, indicating a stronger pinning effect at the higher volume fraction of the second phase. Together, these data establish a direct correlation between the microstructure, Ce content, and the sintering atmosphere.

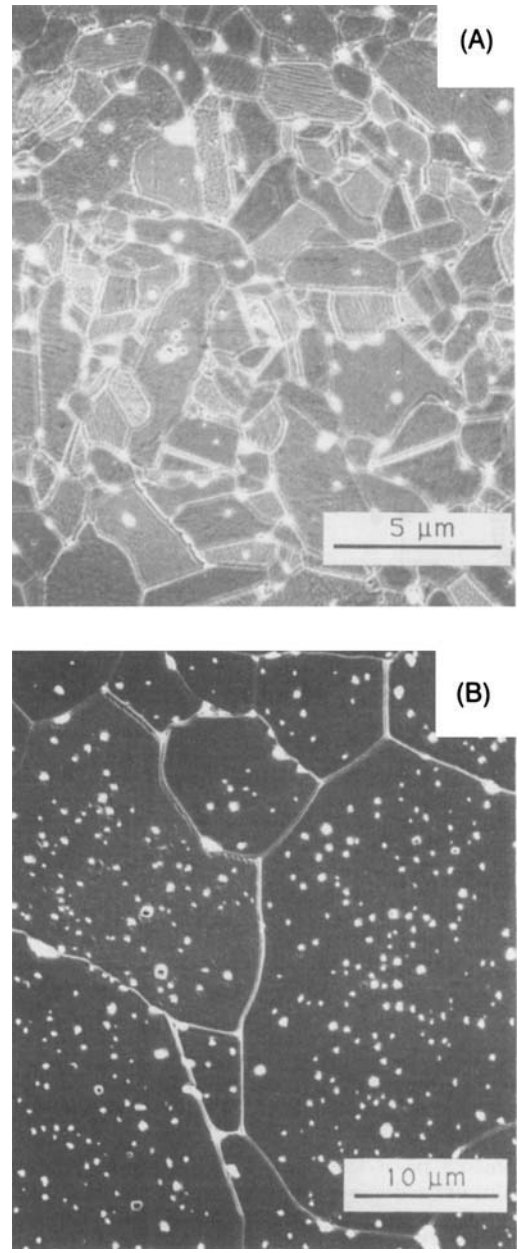

Fig. 2. SEM micrographs of sample 98A/2Zr3Ce sintered at 1550°C for 4 h in (A) air, and (B) hydrogen.

The large effect of Ce doping and sintering atmosphere on the alumina grain size became more prominent after a breakaway transition in the microstructure. The initial microstructures, e.g., after 30 min sintering, of the two samples shown in Fig. 2 were actually similar. Subsequently, the grain boundary broke away from second-phase particles in the hydrogen-sintered sample at about 1 h sintering time. To document this transition, the alumina grain size and zirconia particle size as a function of sintering time for samples 98A/2Zr1Ce, 98A/2Zr3Ce, and 98A/2Zr10Ce, sintering in hydrogen, are shown in Fig. 5. The approximate sintering times at which the boundary–particle breakaway occurred are indicated in the plot. As can be seen, at the lowest Ce doping level (98A/2Zr1Ce), the breakaway initiated at the longest sintering time (nearly 4 h), while at higher Ce contents (98A/2Zr3Ce and 98A/2Zr10Ce) the breakaway occurred sooner, in less than 1 h. This is in contrast to the air-sintered samples already shown in Fig. 3, in which no breakaway was observed at all times.

As the pinning effect of the second phase increases, at higher ZrO_2 volume fractions, the breakaway transition is

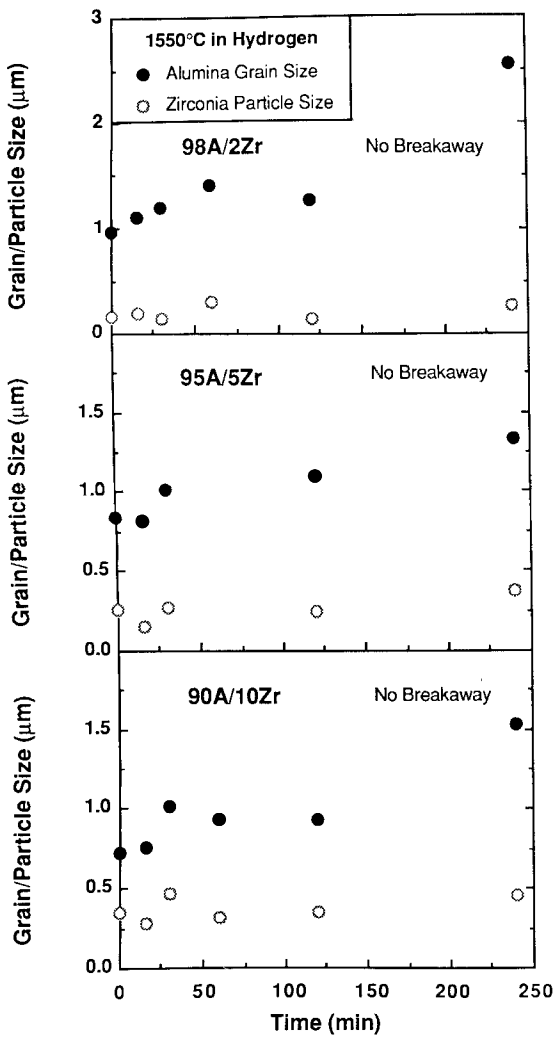

Fig. 3. Alumina grain size and zirconia particle size as a function of sintering time for three undoped composites containing 2, 5, and 10 vol% ZrO_2 sintered at 1550°C for 4 h in hydrogen.

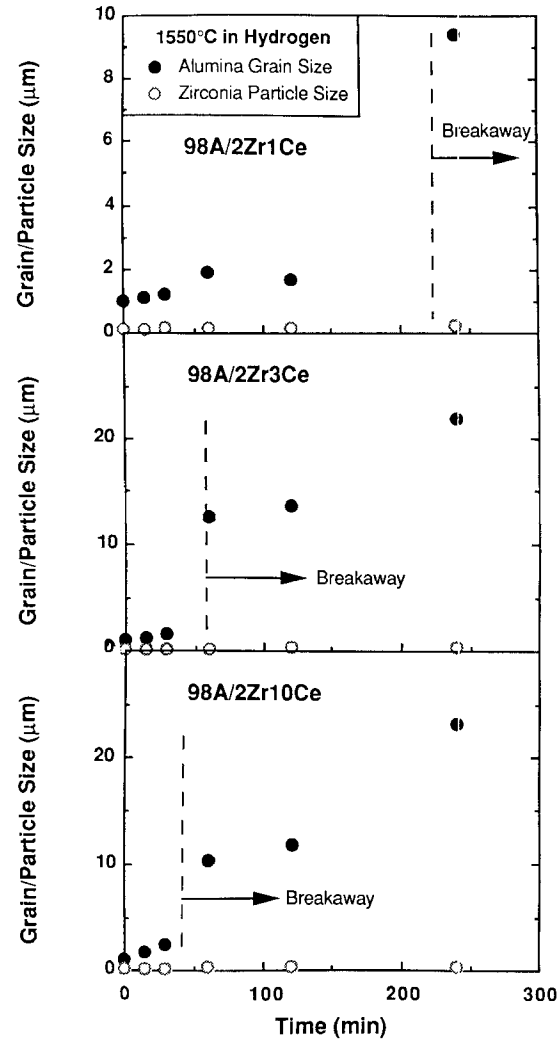

Fig. 5. Alumina grain size and zirconia particle size as a function of sintering time for three 2 vol% ZrO_2 composites of different cerium content sintered at 1550°C in hydrogen.

suppressed or at least postponed and may require a larger amount of Ce doping. Figure 6 summarizes alumina grain size and zirconia particle size data during hydrogen sintering for 90A/10Zr1Ce, 90A/10Zr3Ce, and 90A/10Zr10Ce. No breakaway occurred for the first two compositions, but it did take place for the last one. Figure 7 shows the microstructures of 90A/10Zr10Ce sintered in air and in hydrogen for 4 h. While the contrast in these microstructures is evident and

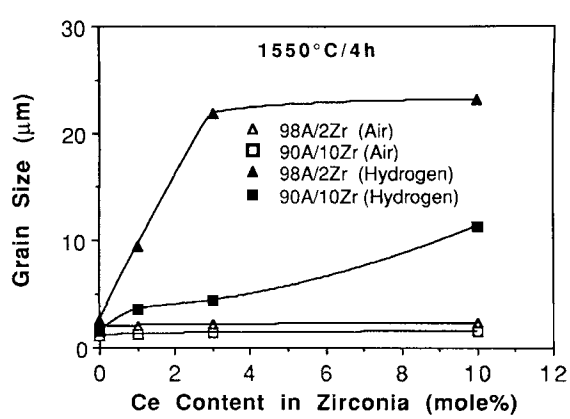

Fig. 4. Cerium content dependence of alumina grain size for composites containing 2 and 10 vol% ZrO_2 sintered at 1550°C for 4 h in either air or hydrogen.

many intragranular ZrO_2 particles can be clearly seen in the hydrogen-sintered sample, the breakaway microstructure is more restrained than that obtained at a lower particle fraction, e.g., Fig. 2(B). The intermediate case, with 5 vol% second-phase particles, is shown in Fig. 8 for comparison. They are quite similar to Fig. 2 except for different grain sizes in the case of hydrogen sintering. These data are summarized in a grain size and particle size plot for all the specimens sintered in hydrogen at 1550°C in Fig. 9, where open symbols are for microstructures before the breakaway transition and full symbols after the transition.

(2) Breakaway Transition with and without ZrO_2

In order to further isolate the cation species responsible for the breakaway transition, we have investigated a series of compositions, 95A/5Zr*m*Ce where *m* ranges from 0 to 100. They were sintered in either air or hydrogen for 4 h under processing conditions similar to those used before. All samples sintered to a relative density of >98%. In the limit of $m = 100$, we have substituted zirconia by ceria entirely and thus the sample contains no ZrO_2. Data of alumina grain size of this series are shown in Fig. 10. In air sintering, no breakaway was observed, and the grain size is uniformly small. In hydrogen sintering, however, breakaway always occurred when the ceria content was higher than 3 mol% and remained so all the way up to 100 mol% ceria substitution. The average grain size as can be noted in this case actually decreased somewhat at higher ceria substitution. This de-

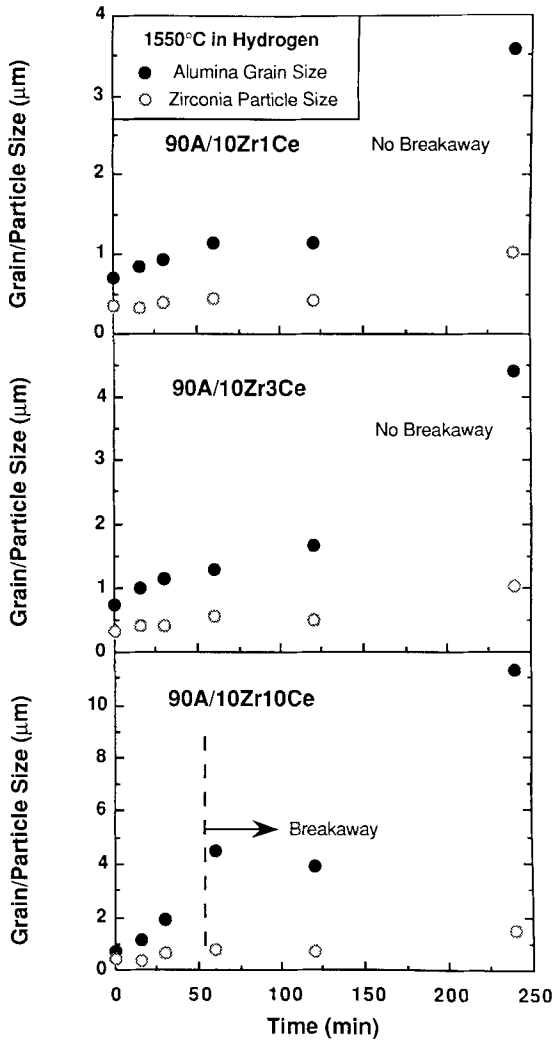

Fig. 6. Alumina grain size and zirconia particle size as a function of sintering time for three 10 vol% ZrO_2 composites of different cerium content sintered at 1550°C in hydrogen.

creasing in average grain size was not fully understood and was not further investigated in our study. However, one may speculate that it might be attributed to possibly lower sinterabilities of the higher ceria content samples, which would result in a shorter effective grain growth time. The conclusion drawn from these data is that the presence of zirconia is not a necessary condition for the breakaway. We also reconfirm that a certain amount of Ce, in this case 3 mol% on the basis of Zr + Ce, is required for the breakaway. This doping level of 3 mol% coincides with the solubility limit of Ce^{3+} in ZrO_2.[12,13,16]

(3) Alumina with M^{3+} Dopants with and without ZrO_2

In hydrogen sintering, Ce is believed to be in the trivalent state. To simulate this situation, we have investigated the effect of several trivalent dopants which have ionic radii comparable to Ce^{3+}. Single-phase alumina samples were prepared under processing conditions similar to the ones described in Section II, including attrition milling. These samples contained no zirconia but included 200 ppm of various dopants (Ce, Y, and La). Sintering was performed in either air or hydrogen, and the resultant microstructures were compared. All these samples reached relative densities >98% within the first 30 min of the sintering at 1550°C. As shown in Fig. 11, the grain size of undoped alumina processed in this way has a grain size of ~4 μm if sintered in air and ~5 μm if sintered in hydrogen. The grain size of Ce-doped alumina is sensitive to the sintering atmosphere and is much smaller in air than in hydrogen. Most significantly, the grain size of Y^{3+} and La^{3+}

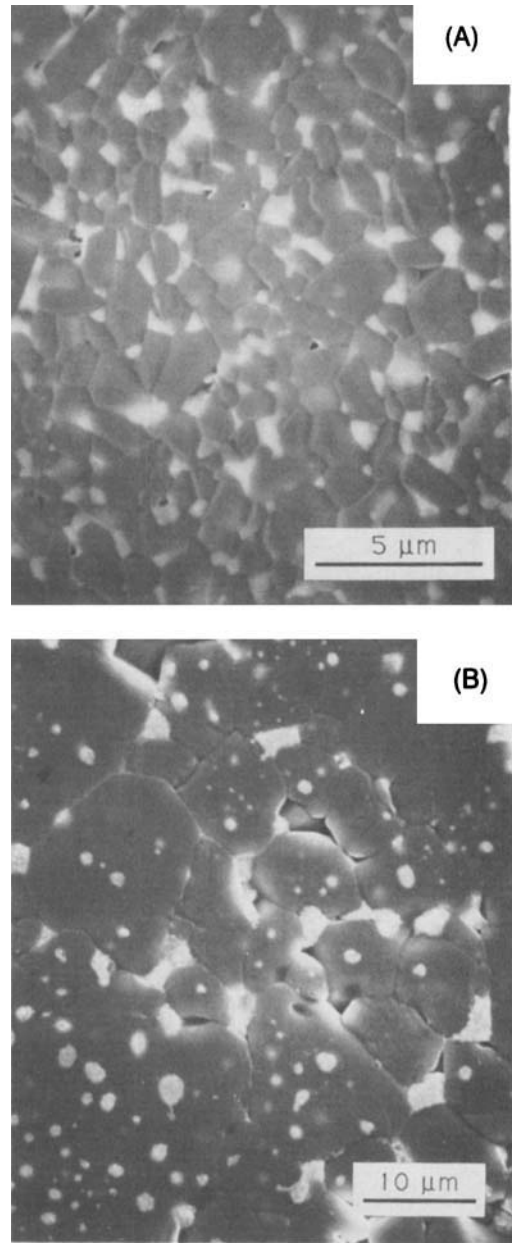

Fig. 7. SEM micrographs of sample 90A/10Zr10Ce sintered at 1550°C for 4 h in (A) air and (B) hydrogen.

doped alumina is not sensitive to the atmosphere and is much larger than that of undoped alumina. Thus, all three trivalent dopants, Y^{3+}, Ce^{3+}, and La^{3+}, can enhance grain growth in alumina.

We have also examined the microstructures of a series of alumina/zirconia composites (ZTA) containing 2 and 10 vol% ZrO_2, which are further doped with La or Y at a level of 1 mol% on the basis of Zr + M, using similar processing methods described in the previous section. Breakaway transition was not observed at this doping level in any of these samples, and the average grain sizes were all small (3 to 5 μm). These observations indicate that the presence of zirconia suppresses the grain growth enhanced by M^{3+} doping. Apparently, the reason for no breakaway observed here is the low doping level (1 mol%) of the M^{3+} as compared to their solid solubilities (>10 mol%) in ZrO_2.[20,21] This issue will be discussed in Section IV(2).

(4) High-Purity Alumina without Processing Contamination

To further isolate the source of grain growth enhancement, we have studied a series of high-purity alumina, with or with-

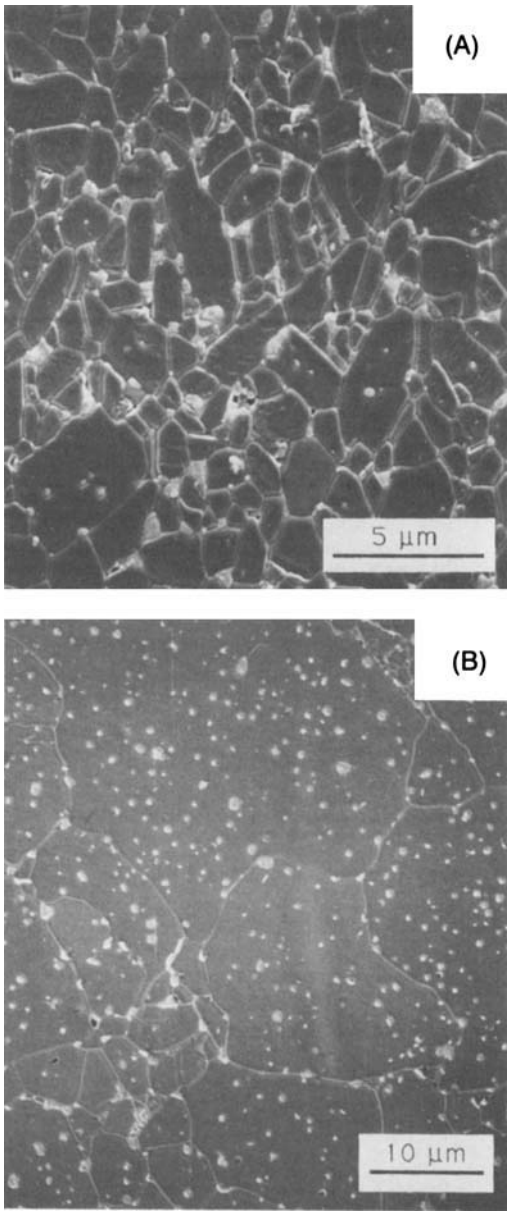

Fig. 8. SEM micrographs of sample 95A/5Zr10Ce sintered at 1550°C for 4 h in (A) air and (B) hydrogen.

out dopants, which were processed without attrition milling. We also eliminated the step of pressure casting from processing, and used die pressing and cold isostatic pressing only. The use of glassware was completely avoided during the entire processing. This relatively clean process is expected to greatly reduce accidental contamination, especially the amount of glassy (silica) phase in the sintered alumina. The grain growth data from this series of alumina are presented in Fig. 12. The results show that all the samples now have comparable grain size, regardless of the type of dopant (La^{3+} and Ce^{3+}) and sintering atmosphere. The codoping of 400- and 2000-ppm zirconia with ceria in the study did not produce any synergistic effect, either. It is finally noted that the grain size of the undoped alumina is slightly larger in hydrogen sintering (~5 μm) than in air sintering (~4 μm), and in both cases it is similar to that shown in Fig. 11, for the case containing some silica contamination. Thus, while grain growth in "pure" alumina is not too sensitive to silica contamination, in all other trivalent-cation-doped aluminas it is.

(5) Ce Distribution

To determine the location of Ce ions, a qualitative energy-dispersive X-ray analysis (EDAX) composition analysis was performed on a 90A/10Zr3Ce specimen. The sample was sintered at 1550°C in hydrogen for 2 h, then quickly cooled to room temperature in a flow of hydrogen. When the analysis was conducted over a large area containing both alumina grains and zirconia second-phase particles, no cerium was detected. This is not unexpected, because the average concentration of cerium, being ~0.3% in this case, was below the detectability (~1%) of the instrument. Neither was any cerium detected when the electron beam was focused over areas of alumina grains without ZrO_2 particles. However, when the electron beam was focused on individual zirconia particles, cerium was found in the analysis even though the actual area analyzed in the latter case (considering beam broadening and the large excitation volume of X-ray underneath the specimen surface) was still several times larger than that of a single submicrometer zirconia particle. The above result strongly

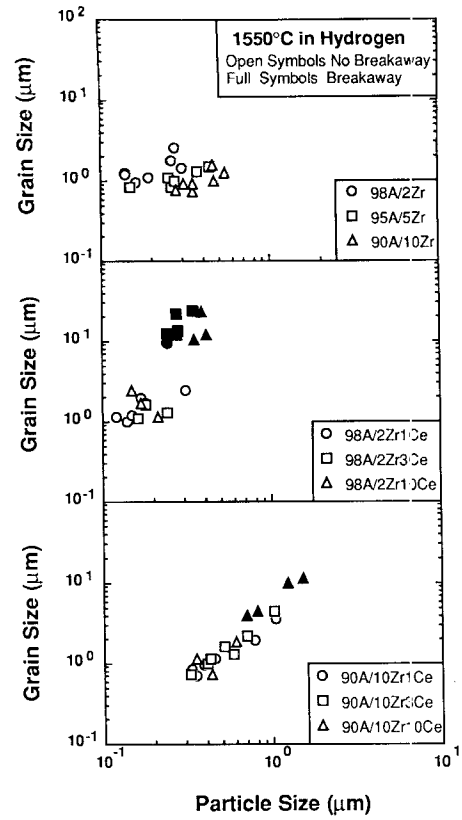

Fig. 9. Grain-size–particle-size relationship for several ZTA's sintered in hydrogen at 1550°C. Full symbols indicate a breakaway microstructure was observed.

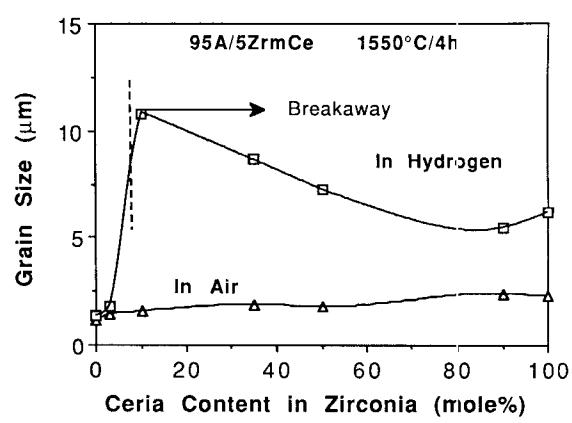

Fig. 10. Grain size as a function of ceria content for 95 vol% alumina and 5 vol% zirconia/ceria sintered at 1550°C for 4 h in either air or hydrogen.

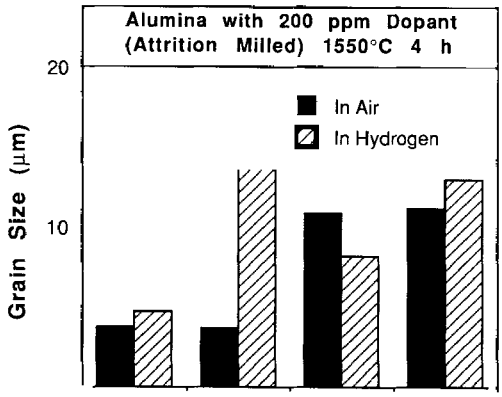

Fig. 11. Grain size of doped alumina (at 200 ppm) sintered at 1550°C for 4 h in either air or hydrogen.

suggests that, in hydrogen sintering, Ce^{3+} in 90A/10Zr3Ce is mostly associated with zirconia. (In air, Ce association with ZrO_2 is virtually guaranteed by the very large solubility of Ce^{4+}.)

IV. Discussion

The experimental observations can be briefly summarized as follows:

(1) When processing-related contamination is eliminated, Y^{3+}, La^{3+}, Ce^{3+}, Ce^{4+}, and Zr^{4+} do not significantly enhance grain growth of alumina.

(3) In case (2) and with additional zirconia present, Ce^{3+} can enhance grain growth if its concentration is greater than 3% (its solubility limit), on the basis of Zr + Ce, resulting in breakaway of zirconia particles from grain boundary; Ce^{4+} does not and Y^{3+} and La^{3+} at a concentration of 1% do not.

(4) In zirconia-added alumina, Ce^{3+} is concentrated in zirconia particles.

We believe that the above observations support the following statements:

(1) The enhancing effect of M^{3+} on grain growth is associated with the glassy phase on the grain boundary which forms from silica contamination during processing.

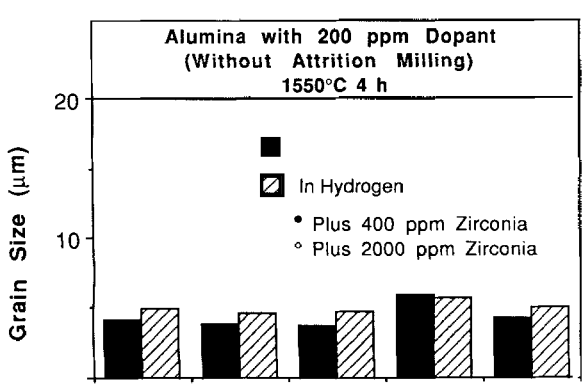

Fig. 12. Grain size of high-purity alumina sintered at 1550°C for 4 h in either air or hydrogen.

(2) Zirconia has a scavenging effect on M^{3+} at low M concentrations so that M^{3+} can enhance grain growth and cause the breakaway transition only if its solubility limit in zirconia is exceeded.

The role of glassy grain-boundary phase, the scavenging effect of zirconia, and the mechanism of the breakaway transition are further discussed in the following.

(1) Dopant Effect on Grain-Boundary Glassy Phase

The experimental evidence presented in Figs. 10 and 11 strongly implies that the dopant effect on enhanced grain growth is associated with processing contamination during attrition milling and/or other steps in which glassware was used. It is well-known that such contamination often introduces silica to the ceramic, forming a grain-boundary glassy phase.[7,17] Observations of this kind in alumina/zirconia ceramics have been well documented.[7] Indeed, under normal processing conditions using milling procedures, a continuous grain-boundary glassy phase is almost ubiquitous. In the presence of such a glassy phase, grain-boundary transport is expected to be facilitated, which will in turn enhance grain growth. Dopants that lower the viscosity of the glassy phase can have a major effect on increasing M_b, the grain-boundary mobility. In the present study, we have found that M^{3+} ions in the absence of ZrO_2 have a significant effect on grain growth and thus M_b. This would be explicable if they serve as a flux to lower the glass viscosity (these large trivalent ions with high coordination numbers are known as glass modifiers) and increase the boundary mobility.[18] On the other hand, Ce^{4+} and Zr^{4+} seem to have little effect on M_b. This might be deemed reasonable in view of the low solubility (a few weight percent)[7,19] of Zr^{4+} in the glass and the isoelectric nature of these tetravalent cations in relation to Si^{4+}, making them either glass formers or intermediates but not glass modifiers.[18] In this regard, Al^{3+} ions, which are constituents of the glass (in the order of ~10 wt%),[7] serve also as glass formers.[18]

Our investigation has revealed that the presence of ZrO_2 can suppress the enhancing effect of M^{3+} dopants on grain growth. For example, in 95A/5ZrYCe, there is no enhanced grain growth in hydrogen sintering if $y < 3$. Likewise, in ZTA containing 1 mol% La^{3+} and Y^{3+} dopants, on the basis of La/(Zr + Ce) or Y/(Zr + Y), a uniform microstructure of fine grains was obtained. This can be readily understood by noting the high solubility of M^{3+} cations in zirconia. For instance, the solubility of La^{3+} is 12 mol% and that of Y^{3+} is ~50 mol%.[20,21] In the case of Ce^{3+}, the solubility in zirconia is around 3 mol%,[12,13,16] in coincidence with the minimum concentration required of Ce^{3+} for abnormal grain growth in Fig. 9. Inasmuch as these dopants are tied to zirconia at lower concentrations, they are not expected to be present to any large extent in the glassy phase, hence not affecting grain-boundary mobility.

It is also interesting to question whether ZrO_2 acts as a scavenger for cations other than trivalent ones. For Ce^{4+}, the solubility in ZrO_2 is again high, and ZrO_2 can act as a scavenger (although Ce^{4+} does not seem to enhance M_b in any way). On the other hand, for alkali impurity, ZrO_2 is not expected to act as a scavenger, since its solubility is very low. In the study of Kibbel and Heuer of ZTA,[7] an overall alkali impurities level of only 0.001 wt% was detected, and a breakaway microstructure was still observed. This is consistent with our expectation of no scavenging effect. Overall, the solubility argument seems to have some merit.

The breakaway transition takes place when the grain-boundary velocity exceeds the particle velocity. The ratio of particle mobility to grain-boundary mobility, M_p/M_b, is of special interest here. From theoretical considerations,[4,11] it has been shown that M_p is proportional to D_i/r^4, where D_i is the

interface diffusivity* on the particle/matrix interface, and r is the particle radius. Further considerations have also identified the following breakaway condition:[22]

$$r \geq (C\Omega^{1/3}\delta_i D_i \gamma_i / kTM_b\gamma_b)^{1/2} \quad (1)$$

where Ω is the atomic volume, δ_i is the interface thickness for diffusion, γ_i is interfacial energy, γ_b is the grain-boundary energy, kT has its usual meaning, and C is a dimensionless function whose form is model dependent but is only weakly dependent on the ratio of grain size to particle size, if at all. Thus, the most relevant factors affecting the breakaway transition are M_b, r, and D_i.

Our data of grain size and particle size summarized in Fig. 9 are partly consistent with Eq. (1), in that the breakaway transition occurs when the particle size exceeds a certain value. The critical particle size, however, is dependent on the volume fraction of the second phase, as evident from a comparison of the breakaway point in samples containing 2 and 10 vol% ZrO_2. Thus, granting the dependence on M_b, r, and D_i in Eq. (1) to be correct, it is at least necessary to incorporate dependence of particle volume fraction into the dimensionless function C in the above equation. The following discussion is based on this modified interpretation of Eq. (1).

It is obvious in our experiments that M_b has been significantly enhanced by the addition of M^{3+} cations. Judging from the data of Fig. 11, in which the alumina grain size varies by a factor of 3.5 from the case of Ce^{4+} doping to Ce^{3+} doping, we may estimate an enhancement factor of $(3.5)^2$, or 12, for M_b. This will have an effect of decreasing the critical particle size by a factor of 3.5, provided interfacial diffusivity of alumina remains unchanged. Since Ce^{3+} doping at different levels will probably affect M_b monotonically, we should expect the critical particle size at the breakaway transition to decrease monotonically with the Ce^{3+} concentration. This expectation is supported by the limited data in Fig. 9. For example, at 2 vol% ZrO_2, the maximum particle size recorded before breakaway increased from 0.21 μm for 98A/2Zr10Ce, to 0.25 μm for 98A/2Zr3Ce, to 0.3 μm for 98A/2Zr1Ce. The same comparison for the 10 vol% ZrO_2 samples is also satisfactory: the breakaway occurred in 90A/10Zr10Ce at a particle size of 0.65 μm and did not occur in either 90A/10Zr3Ce or 90A/10Zr1Ce at a particle size larger than 1.1 μm. Using these data as a reference, it is also clear that, without Ce^{3+}, the maximum particle size recorded for 98A/2Zr at 0.29 μm, and for 90A/10Zr at 0.55 μm, is not sufficient for triggering the breakaway transition, considering the lower M_b in these undoped materials. In short, our observations of the breakaway transition can be qualitatively understood on the basis of the doping effect on M_b alone. (Ce^{3+} doping can also influence the breakaway condition through the change of grain-boundary energy. However, it is highly unlikely that a slight change in boundary glass composition will result in an order of magnitude increase in boundary energy, which would be needed to explain the experimental data.)

In the above discussion, we have left the role of D_i unexplained. Our experimental data do not provide any direct probe into the magnitude of D_i nor its variation with doping. However, since Eq. (1) depends on the ratio of M_b to D_i only, we may suggest that it is M_b/D_i (or M_b/M_p at a constant particle size) that monotonically increases with Ce^{3+} doping. It is noted that in both M_b and D_i, it is alumina transport, controlled either by Al diffusion or O diffusion, that is pertinent. Since Al diffusion along the grain boundary is slower than that of O, M_b is probably controlled by Al diffusion.[23] On the other hand, since O diffusion across ZrO_2 is expected to be very fast, via either lattice or interface boundary, D_i is probably also controlled by Al diffusion. Thus, our data suggest that, during Ce^{3+} doping, Al diffusion along the Al_2O_3 grain boundary is enhanced to a larger extent than that along the ZrO_2/Al_2O_3 interface.

In a recent review of our data and the literature on diffusional creep of fine-grained alumina, which is controlled by Al diffusion along grain boundary, we have pointed out that the addition of a small amount of ZrO_2 to Al_2O_3 can dramatically lower the creep rate of the latter.[24] For example, although "pure" alumina at a comparable grain size deforms at about the same rate as tetragonal zirconia stabilized by 2 mol% Y_2O_3, which is a well-known superplastic ceramic, alumina in an alumina/zirconia composite is considerably hardened and behaves essentially like a rigid phase. Although the mechanistic origin of the above phenomenon remains to be elucidated, we may speculate that the ZrO_2/Al_2O_3 interface is somehow "poisoned" and not capable of providing an adequate source/sink action for Al diffusion as measured by D_i In diffusional creep, this effect is apparently independent of the addition of other trivalent dopant cations, such as Y^{3+}. Thus, by analogy, we may expect Ce^{3+} doping to have little effect on D_i. If the above reasoning proves correct, the doping effect on the breakaway transition can be explained in terms of M_b only.

V. Conclusions

(1) Two distinctively different types of microstructure for alumina/Ce-doped zirconia can be obtained through the control of cerium ion valence.

(2) In the presence of a glassy phase, Ce^{3+} depresses the M_p/M_b ratio by enhancing grain-boundary mobility of alumina through a fluxed glassy boundary phase. Above a certain size, zirconia particles break away from the alumina grain boundary, leaving behind an intragranular ZrO_2 dispersion in an abnormally grown alumina matrix.

(3) Ce^{4+} has little effect on the grain growth of alumina or alumina/zirconia composites.

(4) Trivalent cations, La^{3+} and Y^{3+}, have effects similar to Ce^{3+}.

(5) ZrO_2 acts as a scavenger for trivalent cations, provided their solubility limit in ZrO_2 is not exceeded.

References

[1]C. Zener; private communication to the author. See C.S. Smith, "Grains, Phases, and Interfaces: An Interpretation of Microstructure," *Trans. AIME*, **175**, 15–51 (1948).

[2]R. J. Brook, "Controlled Grain Growth"; pp. 331–64 in *Treatise on Materials Science and Technology*, Vol. 9. Edited by F. F. Wang. Academic Press, New York, 1976.

[3]F. F. Lange and M. M. Hirlinger, "Hindrance of Grain Growth in Al_2O_3 by ZrO_2 Inclusions," *J. Am. Ceram. Soc.*, **67** [3] 164–68 (1984).

[4]P. G. Shewmon, "Movement of Small Inclusions in Solids by a Temperature Gradient," *Trans. Metall. Soc. AIME*, **230** [6] 1134–37 (1964).

[5]R. L. Coble, "Transparent Alumina and Method of Preparation," U.S. Pat. No. 3026210, March 20, 1962.

[6]R. L. Coble, H. Song, R. J. Brook, C. A. Handwerker, and J. M. Dynys, "Sintering and Grain Growth in Alumina and Magnesia"; pp. 839–52 in Advances in Ceramics, Vol. 10 *Structure and Properties of MgO and Al_2O_3 Ceramics*. Edited by W. D. Kingery. American Ceramic Society, Columbus, OH, 1984.

[7]B.W. Kibbel and A. H. Heuer, "Exaggerated Grain Growth in ZrO_2-Toughened Al_2O_3," *J. Am. Ceram. Soc.*, **69** [3] 231–36 (1986).

[8]D. J. Green, "Critical Microstructures for Microcracking in Al_2O_3–ZrO_2 Composites," *J. Am. Ceram. Soc.*, **65** [12] 610–14 (1982).

[9]J.-T. Lin and H.-Y. Lu, "Grain Growth Inhibition and Mechanical Property Enhancement by Adding ZrO_2 to Al_2O_3 Matrix," *Ceram. Int.*, **14**, 251–58 (1988).

[10]S. Hori, R. Kurita, M. Yoshimura, and S. Somiya, "Influence of Small ZrO_2 Additions on the Microstructure and Mechanical Properties of Al_2O_3"; pp. 423–29 in Advances in Ceramics, Vol. 24, *Science and Technology of Zirconia III*. Edited by S. Somiya, N. Yamamoto, and H. Hanagida. American Ceramic Society, Westerville, OH, 1988.

[11]B.W. Kibbel and A. H. Heuer, "Ripening of Inter- and Intragranular ZrO_2 Particles in ZrO_2-Toughened Al_2O_3"; pp. 415–24 in Advances in Ceramics, Vol. 12, *Science and Technology of Zirconia II*. Edited by N. Claussen, M. Ruhle, and A. H. Heuer. American Ceramic Society, Columbus, OH, 1984.

[12]A. I. Leonov, A. B. Andreeva, and E. K. Keler, "Influence of the Gas

*For particle migration, as for pore migration, it is the mass transport of the matrix substance which is necessary.

Atmosphere on the Reaction of Zirconium Dioxide with Oxides of Cerium," *Izv. Akad. Nauk SSSR, Neorg. Mater.*, **2** [1] 137–44 (1966).

[13]M. Yoshimura and T. Sata, "Phase Studies on the System ZrO_2–Ce_2O_3 from 1350°C to 1900°C," *Bull. Tokyo Inst. Technol.*, **108**, 25–32 (1972).

[14]L. A. Xue and I-W. Chen, "Deformation and Grain Growth of Low-Temperature-Sintered High-Purity Alumina," *J. Am. Ceram. Soc.*, **73** [11] 3518–21 (1990).

[15]J. C. Wurst and J. A. Nelson, "Lineal Intercept Technique for Measuring Grain Size in Two-Phase Polycrystalline Ceramics," *J. Am. Ceram. Soc.*, **55** [2] 109 (1972).

[16]K.-H. Heussner and N. Claussen, "Strengthening of Ceria-Doped Tetragonal Zirconia Polycrystals by Reduction-Induced Phase Transformation," *J. Am. Ceram. Soc.*, **72** [6] 1044–46 (1989).

[17]S. J. Bennison and M. P. Harmer, "Grain Growth Kinetics for Alumina in the Absence of a Liquid Phase," *J. Am. Ceram. Soc.*, **68** [1] C-22–C-24 (1985).

[18]W. D. Kingery, H. K. Bowen, and D. R. Uhlmann, *Introduction to Ceramics*, 2nd ed.; Ch. 3 and 14 (pp. 91–124 and 704–67). Wiley, New York, 1976.

[19]E. M. Levin, C. R. Robbins, and H. F. McMurdie; Fig. 772 in *Phase Diagrams for Ceramists*. Edited by M. K. Reser. The American Ceramic Society, Columbus, OH, 1964.

[20]See Ref. 19, Fig. 346.

[21]E. M. Levin and H. F. McMurdie, Fig. 4437 in *Phase Diagrams for Ceramists (1975 Supplement)*. Edited by M. K. Reser. The American Ceramic Society, Columbus, OH, 1975.

[22]C. H. Hsueh, A. G. Evans, and R. L. Coble, "Microstructure Development During Final/Intermediate Stage Sintering–Pore/Grain Boundary Separation," *Acta Metall.*, **30** [7] 1269–79 (1982).

[23]A. E. Paladino and R. L. Coble, "Effect of Grain Boundaries on Diffusion-Controlled Processes in Aluminum Oxide," *J. Am. Ceram. Soc.*, **46** [3] 133–36 (1963).

[24]I-W. Chen and L. A. Xue, "Development of Superplastic Structural Ceramics," *J. Am. Ceram. Soc.*, **73** [9] 2585–609 (1990). □